Jurnal Kejuruteraan 38(3) 2026: 1173-1186
https://doi.org/10.17576/jkukm-2026-38(3)-14

Integration of Aerial Photogrammetry, UAV LiDAR and Terrestrial LiDAR Point Clouds for Individual Tree Measurement and Individual Tree Carbon Storage Estimation

Omar Farouk Fauzi[a], Muhammad Zulkarnain Abd Rahman[a*], Alvin Lau Meng Shin[a], Wan Hazli Wan Kadir[a], Mohd Faisal Abdul Khanan[a], Mohd Radhie Mohd Salleh[c], Hamdan Omar[b], Muhammad Safwan Ruslan[a], Puven Raj P. Chazian[a], Mohd Asraff Asmadi[a] & Muhammad Khalid[d]

[a]*Department of Geoinformation, Faculty of Built Environment and Surveying, Universiti Teknologi Malaysia, 81310 Johor Bahru, Johor, Malaysia*

[b]*Geoinformation Programme, Division of Forestry and Environment, Forest Research Institute Malaysia, Selangor 52109, Malaysia*

[c]*Hydraulics and Hydrology Research Group, Faculty of Civil Engineering, Universiti Teknologi Malaysia, 81310 Johor Bahru, Johor, Malaysia*

[d]*School of Geography and Information Engineering, China University of Geosciences, 430074, Wuhan, China*

[*]*Corresponding author: mdzulkarnain@utm.my*

Received 14 July 2025, Received in revised form 9 January 2026
Accepted 9 February 2026, Available online 30 May 2026

ABSTRACT

Urban forest carbon sequestration is vital for environmental health, climate change mitigation, and enhancing the quality of life in urban areas. This paper presents a framework for high density point clouds production by integrating point data from aerial photogrammetry, UAV-based LiDAR and terrestrial LiDAR for individual tree measurements and carbon storage estimation. The aerial photos, UAV-based LiDAR and terrestrial LiDAR were observed based on common ground control points and combined using Iterative Closest Point (ICP) algorithm. The combined point cloud was iltered to separate ground points and normalized based on Digital Terrain Model (DTM). The normalized point cloud was used for individual tree segmentation from which individual tree measurements such as, tree height, Diameter at Breast Height (DBH) and crown diameter were estimated. The estimated tree parameters were used for individual carbon estimation. The results show that the individual tree segmentation method signi icantly underestimated the number of trees. The estimation of DBH, tree height, and crown diameter achieved the Root Mean Square Error (RMSE) value of 0.107m, 1.385m and 2.650m respectively. However, in general the estimates experience underestimation as shown by Mean Bias Error (MBE) with 0.003m, -0.636m and 0.001m for DBH, tree height and crown diameter respectively. The estimated values for each individual tree were used for individual tree biomass and carbon storage recording the Root Mean Square Error (RMSE) at 1970.236 kg and 886.606 kgC respectively while attaining the Mean Bias Error (MBE) measure of 140.019 kg and 63.009 kgC each. The proposed framework showed promising results for individual tree carbon estimation. Nonetheless, further attention should be given on individual tree delineation process.

Keywords: LiDAR; individual tree segmentation; point cloud data integration; individual tree measurement

INTRODUCTION

Conventional forest inventory techniques involve direct measurements and observation. It is commonly sampled within a designated plot with various sizes and shapes allowing access to invaluable insights on the biophysical metrics of the plot. Nevertheless, the direct method of forest inventory is weighed down by its time-consuming and labour-intensive nature (Kleinn et al. 2020; Sibona et al. 2016). Geospatial technology such as Light Detection and Ranging (LiDAR) generates dense point clouds, significantly improving the efficiency of forest data

collection. Present LiDAR technologies, such as terrestrial laser scanners and UAV-based LiDAR have the means to collect detailed forest characteristics with at least a point cloud density of 20 points per square meter. As a result, complex tree structures are extracted precisely (Chen et al. 2018; Gupta et al. 2020). In addition, point cloud individual tree delineation is a process that entails organizing data into meaningful regions of the point cloud. Examples of these algorithms include methods such as region expansion, mean shift, and hierarchical approaches (Bello et al. 2020; Paris et al. 2015; Tao et al. 2015; Yan et al. 2018). The segmented parts of point clouds can be utilized for various tree metrics calculations (Liu et al. 2018; Wieser et al. 2017). Although the direct and conventional methods are meticulous, they are laborious when compared to the geospatial approach.

The study was carried out in response to the limitations of previous studies on forest-related applications. One of the problems that causes the need for this study is the rapid data collection of LiDAR technology. An accurate forest inventory is essential for forestry and ecological management, particularly in an urban setting. The traditional approach requires measurements using measuring tools. In the long term, this method of forest inventory can be time-consuming and susceptible to inconsistencies caused by human mistakes, further compromising the credibility and accuracy of the results (Paudel et al. 2021; Ramezani & Ramezani, 2021). LiDAR technology, such as a terrestrial laser scanner (TLS) and UAV-based LiDAR offer a quick solution that possesses a rapid and accurate ability to obtain data points. Nevertheless, terrestrial laser scanner (TLS) measurements have limited accuracy in estimating tree height. It experiences underestimation due to occlusion and scanner range limitations. UAV-based LiDAR and aerial photogrammetry point clouds may remedy this issue by providing the top view of the tree crown alongside a close-range perspective from a terrestrial laser scanner (TLS), suggesting the integration of these datasets (Cabo et al. 2018; Hartley et al. 2022; Srinivasan et al. 2015). Next, individual tree segmentation on point cloud data enables individual tree measurement extraction, reducing human intervention (Moroni et al. 2014). However, the complex structure of tree branches may come up as an issue in the accuracy of individual tree delineation and will then result in inaccuracies in individual tree measurement due to misdelineations (Krisanski et al. 2021; Zhang et al. 2022).

RELATED WORKS

The essence of geospatial data integration is to overcome the constraints of several data sources. Terrestrial laser scanner (TLS) systems promote a comprehensive point cloud dataset. However, it faces a challenge in accurately estimating tree height due to interference from the crown structure, obstructing light waves and leading to a consequent underestimation (Srinivasan et al. 2015). Meanwhile, UAV-based LiDAR and aerial photogrammetry data provide superior precision in measuring canopies and individual tree heights. Yet, it has an opposite property to terrestrial laser scanners (TLS), where it encounters difficulties when dealing with dense lower canopies (Goldbergs et al. 2018; Wang et al. 2016). Merging multiple point clouds may improve the precision of tree height measurements (Hilker et al. 2010; Zhang et al. 2015).

The conventional method of forest inventory involves intensive fieldwork, including the use of clinometers, diameter tapes, and hypsometers, also known as laser range finders. Sampling can be done with or without the designation of plots or various shapes and sizes. Diameter at breast height (DBH) is measured at 4.5 feet (1.3 to 1.4 meters) from the ground. In terms of forestry, this measurement serves its importance in the estimation of tree growth, size, and volume (Wolter et al. 2012). Diameter at breast height (DBH) is typically measured using diameter tapes or tree callipers. Meanwhile, crown diameter is usually measured along the longest axis of the tree spread supplemented by GNSS receivers. Larjavaara and Muller-Landau (2013) propose the tree height to be measured by a laser range finder and applying a trigonometric equation to find the final tree height.

Geospatial technologies, especially LiDAR, have gone through advancements for forest inventory studies. For example, individual tree delineation algorithms have been improving with emerging techniques like the point-based approach by Shin et al. Shin et al. (2018) and the "treeseg" method by Burt et al. (2018). The point-based approach segments trees through spacing thresholds, while the "treeseg" algorithm outlines trees with LiDAR data included with spectral information but struggles with sparse data. In the context of individual tree measurement, LiDAR in general faces a struggle in identifying diameter at breast height due to occlusions, but methods such as circle approximation and cylinder fitting with the aid of transformation enhance the accuracy of DBH measurements (Huang et al. 2011; Srinivasan et al. 2015; Wilkinson et al. 2016). While individual tree height is measured through the production of the Digital Surface Model and the Digital Terrain Model (DTM). By subtracting both products, individual tree height is produced (Ganz et al. 2019; Ojoatre et al. 2019). Tree height can also be taken from the bottommost part of a tree to the peak of the tree canopy. Additionally, tree crown diameter can possibly be estimated through regression models and allometric equations (Mooij et al. 2009). UAV-based LiDAR offers direct measurement from an aerial perspective (Jin et al. 2022; Saarinen et al. 2014).

Rapid monitoring of stand biomass is crucial in understanding climate change impacts on forest carbon sinks and implementing mitigation policies (Zeng et al. 2018). Typically, forest biomass and carbon storage are estimated by utilizing allometric equation models. It uses dendrometric measures such as diameter at breast height and tree height. Above ground biomass (AGB) refers to the oven-dried weight of the above ground material of the tree. Carbon stocks are converted by a multiplicative factor of 0.5 (Duncanson et al. 2019).

The main objective is to measure the different measurements of trees, namely tree height, diameter at breast height, and tree crown diameter, and to estimate the biomass and carbon storage of trees. Previous studies only used single source LiDAR scanning. For example, some studies only use TLS to extract physical measurements or use only airborne-based LiDAR for physical measurement extraction, hinting at the lack of investigation into integration among LiDAR sensors. This study will explore more on the integration of different modes of LiDAR. Specifically, terrestrial laser scanning (TLS), UAV-based LiDAR and aerial photogrammetric derive point clouds.

METHODOLOGY

The study's flow consisted of phases such as data acquisition, preprocessing, point cloud delineation, individual tree measurement, and accuracy assessment. The flow is also divided into objectives, with each task parallel to the respective objectives. In the data acquisition phase, data comes from UAV-based LiDAR, aerial photogrammetry, and terrestrial laser scanning (TLS). There are also other parts of the data, such as the establishment of ground control points (GCPs) and control points (CPs) for the georeferencing of data and the field data collection as a reference for the LiDAR-derived data. For the data preprocessing, each point of cloud data will be cleaned, and the outliers and noise will be removed using standard deviation-based thresholds. Buildings were removed to focus only on the vegetation. The cleaned datasets are then integrated into a single point cloud, where one of the point clouds acts as reference data using the iterative closest point (ICP) algorithm. Next, tree delineation is done by applying the point-based algorithm proposed by Li et al. (2012) after carrying out point cloud data normalization. From the segmentation, each tree will extract its tree ID, diameter at breast height, tree height, and crown diameter. Finally, data validation is done by comparing the LiDAR-derived measurements with the reference data. Most of the phases were conducted through LiDAR360 software. It possesses the capability to handle forestry-related tasks with its forestry module. Furthermore, the software also contains ICP for multiple point cloud alignment.

DESCRIPTION OF STUDY AREA

The study area (Figure 1) is located at Universiti Teknologi Malaysia (UTM), Skudai, Johor Bahru, Johor, Malaysia. The study area covers a small area since the study focuses on the experimental aspect of tree measurement, and it is possible to test on a handful of vegetation. The centroid of the study area is located at a coordinate of 1°33'28.08" N, 103°38'11.5" E on the WGS84 coordinate system. The topography of the area recorded elevations ranging from 10 to 50 meters. The height of trees within the area is below 30 meters.

FIGURE 1. The study area

GEOSPATIAL DATA COLLECTION

Data acquisition is vital for individual tree delineation and individual tree measurement, encompassing UAV-based LiDAR, terrestrial laser scanning (TLS), and aerial photogrammetry. UAV-based LiDAR was captured using the DJI Matrice 300RTK (SZ DJI Technology Co., Ltd., Shenzhen, China) with the gAirHawk Eagle GS260s (Wuhan Geosun Navigation Technology Co., Ltd., Wuhan, China) as its sensor. The TLS system used was TOPCON GLS 2000 (Topcon Positioning Systems, inc., Japan), providing close-range data. Aerial photogrammetry was performed by DJI Mavic 2 Pro (SZ DJI Technology Co., Ltd., Shenzhen, China), producing raster imagery. Global navigation satellite system (GNSS) receivers (TOPCON HIPER HR AND GR5 (Topcon Positioning Systems, inc., Japan)) are used to carry out ground control point surveys. Consequently, the coordinates can be used for point cloud registration and georeferencing. Consequently, the point cloud data sources can overlay on top of each other. Table 1 summarizes the specifications of the geospatial equipment used in the study.

TABLE 1. Specification of equipments used for geospatial data acquisition.

Equipment	Specifications	Details
TOPCON GLS 2000	Range Resolution	130m
	Scanning Rate	120,000 pts/sec
	Horizontal FOV	360°
	Vertical FOV	270°
	Laser footprint	4mm
	Number of returns	7
gAirHawk Eagle GS260s	Range Resolution	200m
	Scanning frequency	20Hz
	FOV	360°, adjsutable
	Laser line number	20-lines
	Laser Class	905nm class 1 (IEC60825-1:2014)
Mavic 2 zoom	Sensor	1/2.3” CMOS
	FOV	77°
	Aperture	f/2.8 (24mm) – f/3.8 (48mm)
	ISO range	100 – 1600
	Shutter speed	8 - 8/1000s

FIELD DATA COLLECTION

Field data collection was conducted in order to prepare the LiDAR-derived measurement with its reference data for validation of its quality. The diameter at breast height was first measured to be between the heights of 1.3 and 1.4 meters. Using a diameter tape, the diameter is taken for each sampled tree. Meanwhile, tree height is acquired through the use of laser range finders together with the use of a trigonometric equation to produce the final tree height. Individual crown diameter also utilizes the laser range finder to find the longest spread of crown diameter.

GEOSPATIAL DATA PREPROCESSING

The goal of this phase is to convert raw data into usable data for further processing. After forming an orthophoto. Naturally, the product for aerial photogrammetry is produced in the extension “GeoTIFF”. Structure from Motion (SfM) is used for transforming rasters into point clouds, taking advantage of the depth within the imagery. Which then aligns the data type with other point cloud sources in the form of the *.las file format. Raw point clouds often affect the quality of the whole dataset. Noise is eliminated through standard deviation-based thresholds.

POINT CLOUD DATA INTEGRATION

Point cloud data from different sources of LiDAR, including aerial photogrammetric point clouds, UAV-based LiDAR, and TLS are integrated in this phase. The ICP algorithm is used to accurately align multiple point cloud data, leveraging each point cloud’s strengths. The transformation and rotation vectors acquired from point distances are calculated for each iteration and will be applied to all points within the data set (Wang & Zhao, 2017). Figure 2 visualizes the iterative optimization of ICP.

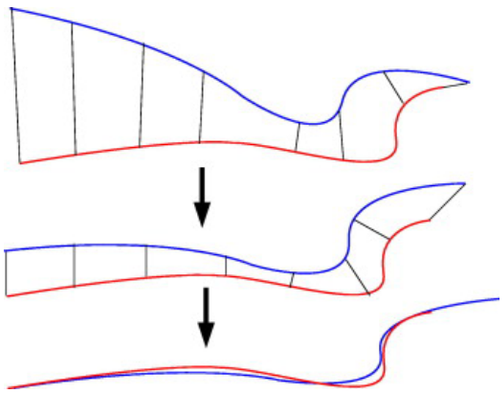

FIGURE 2. Example of alignment optimization while using the ICP algorithm (Smistad et al. 2015).

INDIVIDUAL TREE SEGMENTATION

The integrated point cloud data is delineated into individual trees, highlighting the boundaries between each tree. Each tree delineated will be assigned a unique tree ID with the capability of data storage. As mentioned in the literature review, the point-based method requires the setting of multiple thresholds and parameters, and the algorithm automatically chooses the seed points (Figure 3).

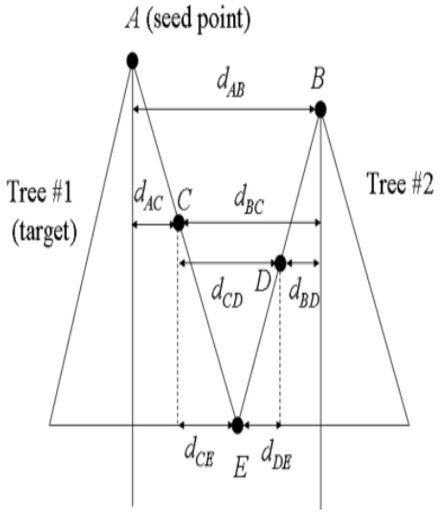

FIGURE 3. Shows a depiction of the point-based algorithm (Li et al. 2012).

To summarize the algorithm, it compares the target points to two of the points that have been segmented. For example, in Figure 3, point E is compared to points C and D. Since point E is closer to point D, we can use the threshold distance of d_{DE}. This may pose a problem since distances may be dynamically changing as the height of trees gets lower and the distance between tree crowns gets closer. The proposed method is to apply an adaptive threshold Shows a depiction of the point-based algorithm (Li et al. 2012).

INDIVIDUAL TREE MEASUREMENT

Tree height is measured from the peak of the canopy to the ground points classified through the triangular irregular network (TIN) densification technique (Zhao et al. 2016), subtracting both heights to get the tree height. Diameter at breast height is measured at 1.3 meters to 1.5 meters above the ground while employing the adaptive circle fitting method to obtain the cross-sectional diameter (Bu & Wang, 2016). The method involves determining an initial radius of DBH and progressively reducing it to fit the tree trunk. Equation 1 and Equation 2 describe the iterative solution for the circle model x_c and r:

$$x_c^{n+1} = \frac{\frac{1}{\sigma_s^2}\frac{1}{P_I^n}\frac{1}{T} P_t^n\left(\left(x_t' - \Delta x_t\right)\right)}{\frac{1}{\sigma_s^2}+\frac{1}{\sigma_c^2}} + \frac{\frac{1}{\sigma_c^2}x_b}{\frac{1}{\sigma_s^2}+\frac{1}{\sigma_c^2}} \quad (1)$$

$$r^{n+1} = \frac{\frac{1}{\sigma_s^2}\frac{1}{P_I^n}\frac{1}{T}\sum_t^T P_t^n\left(\left(x_t' - x_c^n\right)\cos t + \left(\left(y_t' - y_c^n\right)\sin t\right)\right)}{\frac{1}{\sigma_s^2}+\frac{1}{\sigma_r^2}} + \frac{\frac{1}{\sigma_r^2}r_s}{\frac{1}{\sigma_s^2}+\frac{1}{\sigma_r^2}} \quad (2)$$

Where x_c and y_c are the positions of the circle's center, x_t and y_t are the positions of points along the circle parameter, σ is the potential variation in spatial position, center and radius (σ_s, σ_c and σ_t), P is the posterior probability, T represents the point along the circle perimeter and r is the radius of the circle.

Meanwhile, crown diameter is determined by classifying tree crown points and measuring from the horizontal end to another end of the tree crown (Jin et al. 2022).

INDIVIDUAL TREE BIOMASS AND CARBON STOCK ESTIMATION

The tree biomass and carbon stock are commonly estimated by using allometric models. In this case, the allometric model was developed by Ngo and Lum (2018) (Equation 3). It utilizes the measure of DBH to acquire individual tree biomass. Meanwhile, carbon storage is derived from the tree biomass by dividing by its factor of 0.45 (Equation 4) (Lin et al. 2016).

$$\ln(AGB) = 2.511 * \ln(DBH) - 2.413 \quad (3)$$

Where *AGB* is the above ground biomass in kg and *DBH* is the diameter at breast height in cm.

$$Carbon\ Stock = AGB * CF \quad (4)$$

Where *AGB* is the above ground biomass in kg and CF is the conversion factor of 0.5.

ACCURACY ASSESSMENT

Individual tree measurements will undergo quantitative assessment using a series of statistical error metrics. The LiDAR-derived individual tree measurements will be compared to their field-measured counterparts. In this context, the test tools for the accuracy of the tree measurement include the employment of root mean square error (RMSE), coefficient of correlation (r), mean bias error (MBE), and bias to validate the individual tree delineation, which can be found in Equations 5, 6, 7, and 8 respectively.

$$RMSE = \sqrt{\frac{1}{n}\sum_{i=1}^{n}(d_i - D_i)^2} \quad (5)$$

Where RMSE is the root mean square error, n is the number of observations, di is the reference value, and Di is the estimated from LiDAR both at ith number.

$$r = \frac{\sum_{i=1}^{n}(x_i - \bar{x})(y_i - \bar{y})}{\sqrt{\sum_{i=1}^{n}(x_i - \bar{x})^2 (y_i - \bar{y})^2}} \quad (6)$$

Where r is the coefficient of correlation, xi value on the x variable at ith position, $\bar{x}$ is mean value of x, y is the value of the y variable at ith position, and $\bar{y}$ is the mean value of y.

$$MBE = \frac{\sum_{i=1}^{n} d_i - D_i}{n} \quad (7)$$

Where MBE is the mean bias error, di is the actual value Di is the estimated value derived from the LiDAR measurement.

$$Bias = d_i - D_i \quad (8)$$

Where d_i *is* the value of observed measurement, and D_i is the number of predicted at i^{th} count.

RESULTS AND DISCUSSION

This section is divided into several subsections. Notably, data acquisition, point cloud integration, point cloud normalization, individual tree delineation, individual tree measurement, individual tree above ground biomass, and carbon storage estimation.

POINT COUNT AND DENSITY OF DIFFERENT POINT CLOUD DATASET

Point clouds were acquired from three sources. Namely, terrestrial laser scanner (TLS), aerial photogrammetry, and UAV-based LiDAR. Resulting in multiple LAS format files. Each method produces its own unique point cloud densities. Terrestrial laser scanning captured close-range point clouds in "high-speed" mode, emitting 120,000 points per second. 27 stations were set up during the whole TLS survey. The TLS scanning stations were placed and oriented to capture almost every angle of trees within the study area. Terrestrial laser scanning point clouds are then supplemented by UAV-based LiDAR point clouds that help in penetrating through the middle story of the dense crown. However, the point cloud lacks visible colour (RGB), catalyzing point cloud integration. Additionally, an aerial photogrammetric point cloud is generated from an orthophoto that is merged from 352 images. The orthophoto comprises five (5) ground control points, and seven (7) checkpoints. The orthophotos were captured at 60 m above ground level. A dense point cloud is produced using the structure from motion (SfM) technique. Figure 4 visualize the point cloud data captured by each of the stated point cloud sources. Meanwhile, to assess the quality of the point clouds, Table 2 is established to display the point count and density of each point cloud.

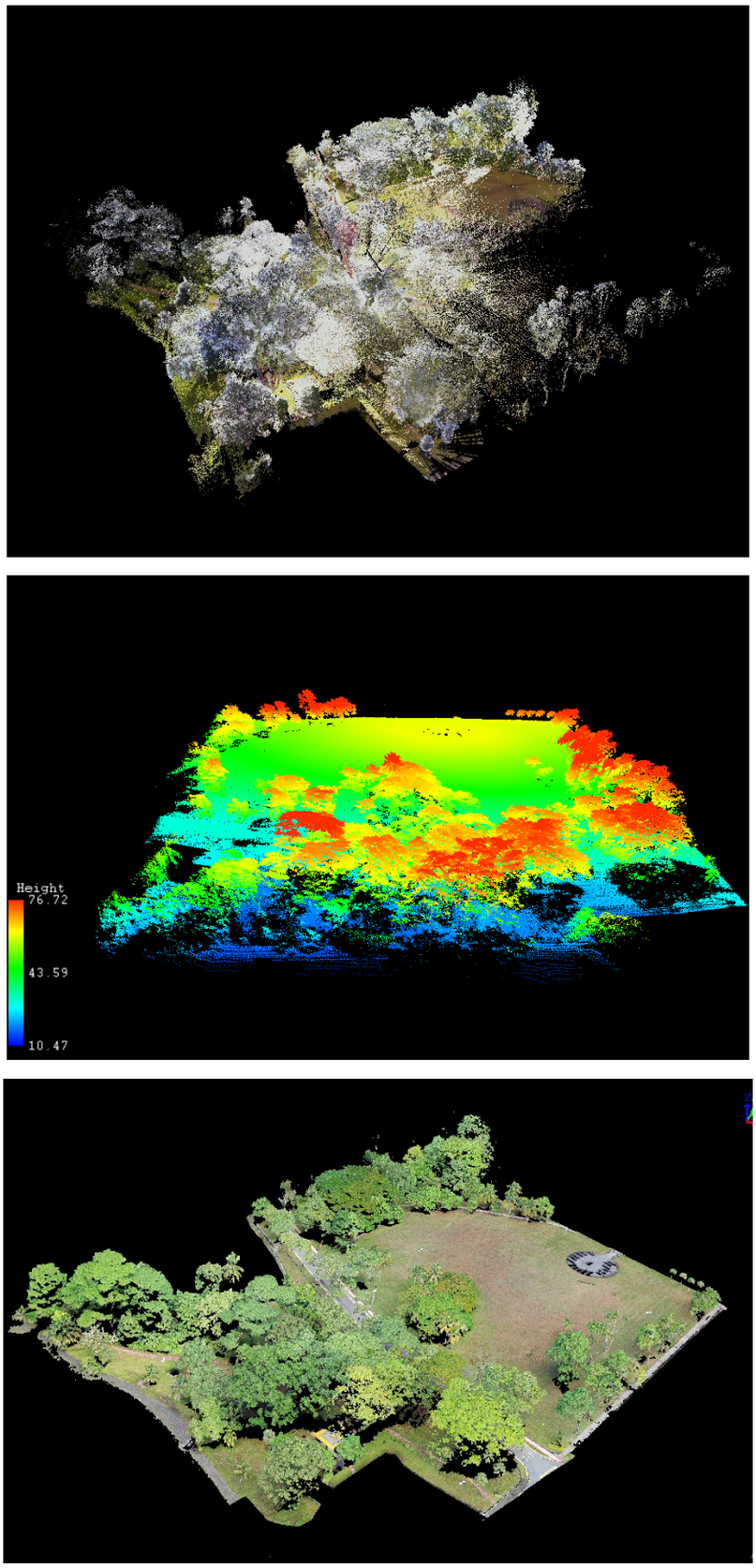

FIGURE 4. Point cloud acquired from (a) terrestrial laser scanning (TLS), (b) UAV-based LiDAR, and (c) Aerial Photogrammetry

TABLE 2. Point count and density of point cloud for the terrestrial laser scanning, UAV-based LiDAR, and aerial photogrammetric point cloud

Types of point cloud data acquistion	Total point count	Covered area (m^2)	Maximum density (pts/m^2)	Average density (pts/m^2)
Terrestrial laser scanner	94,140,028	36,413	226,056	2,585.34
UAV-based LiDAR	2,234,481	32,438	377	68.88
Aerial photogrammetric point cloud	79,192,246	43,200	10,164	1,833.15

Terrestrial laser scanning (TLS) captured the densest point cloud (2585.34 pts/m^2), capturing detailed under-canopy structures while recording an absence of upper-canopy points due to dense foliage. The TLS sensor used has a maximum of seven returns, therefore, after seven layers of stem, it will not register as points. Aerial photogrammetry point clouds helped capture the upper canopy points but struggled at the lower and middle stories of a tree while recording point clouds at a density of 1833.15 pts/m^2. Aerial photogrammetry-derived point cloud basically only have a return number of two. Thus, it explains the irrelevance of aerial photogrammetry as a standalone option for extracting tree measurements. But aerial photogrammetric point cloud provides a detailed representation of point clouds in true colour, which helps visualization. Meanwhile, UAV-based LiDAR has the lowest point cloud density at 68.88 pts/m^2. It effectively penetrated the middle story of trees as well as the upper canopy. However, the points are distributed uniformly across the study area. Nevertheless, each of the sensors displays adequate representation. Terrestrial laser scanning shows a detailed illustration of tree trunks and understory elements due to the close-range nature of the mode. Both UAV-based LiDAR and aerial photogrammetry-derived point cloud excelled at mapping the crown area of individual trees. While UAV-based LiDAR covers decently on the middle story of individual trees, bridging both point clouds from terrestrial laser scanning (TLS) and aerial photogrammetry.

POINT CLOUD DATA INTEGRATION

Point cloud data integration combines point cloud data from terrestrial laser scanning (TLS), aerial photogrammetry, and UAV-based LiDAR into a single, unified dataset. Each of the sensors produces point clouds that are first coarsely registered, followed by fine registration through the Iterative Closest Point (ICP) algorithm, which iteratively minimizes the distance between point clouds. As a result, it achieves an average RMSE of 0.311 m. The RMSE was primarily contributed by the Z component between the TLS, UAV-based LiDAR, and aerial photogrammetry sources. The point clouds were then merged into a unified point cloud. Figure 5 presents the point cloud resulting from the integration process. While Table 3 shows the point count and point cloud density of the integrated point cloud.

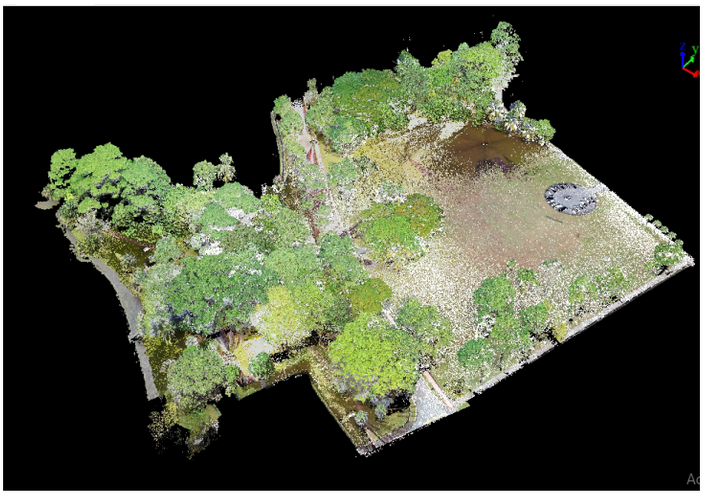

FIGURE 5. Integrated point clouds from terrestrial laser scanning (TLS), UAV-based LiDAR, and aerial photogrammetry.

TABLE 3. Point cloud and point cloud density of integrated point cloud.

Total point count	Covered area (m^2)	Maximum density (pts/m^2)	Average density (pts/m^2)
175,566,755	44,043	222,278	3,986.26

The point clouds acquired were integrated to leverage their individual strengths. Each of the point clouds was roughly aligned using the point cloud registration technique and the iterative closest point (ICP) method to finely align the different point clouds. Consequently, a unified dense point cloud is produced with a density of 3986.26 pts/m^2. As expected, it creates a 360-perspective of the scene within the study area, allowing for a better view of individual trees in a single unified point cloud. The ICP approach accounts for the RMSE at 0.311 m. The TLS survey uses only four initial stations from the aerial photogrammetry to start. The remaining 23 stations were derived from its ranging component. Therefore, misalignment of the point cloud is to be anticipated.

POINT CLOUD NORMALIZATION

Point cloud normalization works by eliminating the original elevation component that has been registered to the local coordinate system and its projection. Ground points are classified prior to the point cloud normalization. The classified ground points act as anchors for the non-ground points. The ground points drag the remaining points nearing an elevation of 0 for their lowest point. It can be explained visually by the example given in Figure 6.

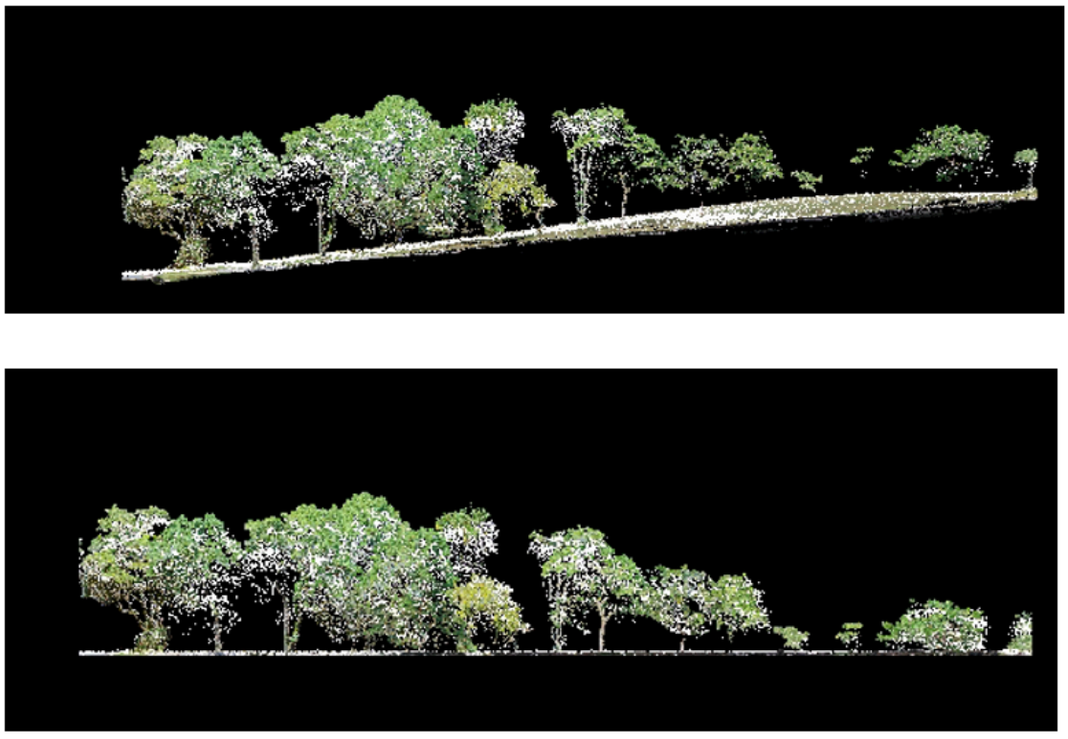

FIGURE 6. (a) Point cloud prior normalization process, and (b) point cloud after normalization process

INDIVIDUAL TREE SEGMENTATION

Individual tree delineation is a method used to distinguish individual trees within a point cloud. The tree delineation is determined by employing seven parameters, which can be reviewed in Each of the parameters plays its own distinct role in tree identification. The parameters involved in the algorithm include minimum cluster size, cluster tolerance, minimum diameter at breast height, height above ground, minimum tree height and trunk height. It requires fine-tuning to avoid overestimation or underestimation. Table 4 shows how the parameters are being set.

TABLE 4. Determined parameters for individual tree delineation

Minimum cluster size (points)	Cluster tolerance (m)	Minimum diameter at breast height (m)	Maximum diameter at breast height (m)	Height above ground (m)	Minimum tree height (m)	Trunk height (m)
1000	0.35	0.1	5	0.3	2	1

As a result, the algorithm outlines each tree according to the seven (7) parameters. Each tree possessed different contrasting colours to differentiate between different delineations. Figure 7 illustrates the result of the individual tree delineation and Table 5 reports on the validation of the delineation through the difference in segmented trees.

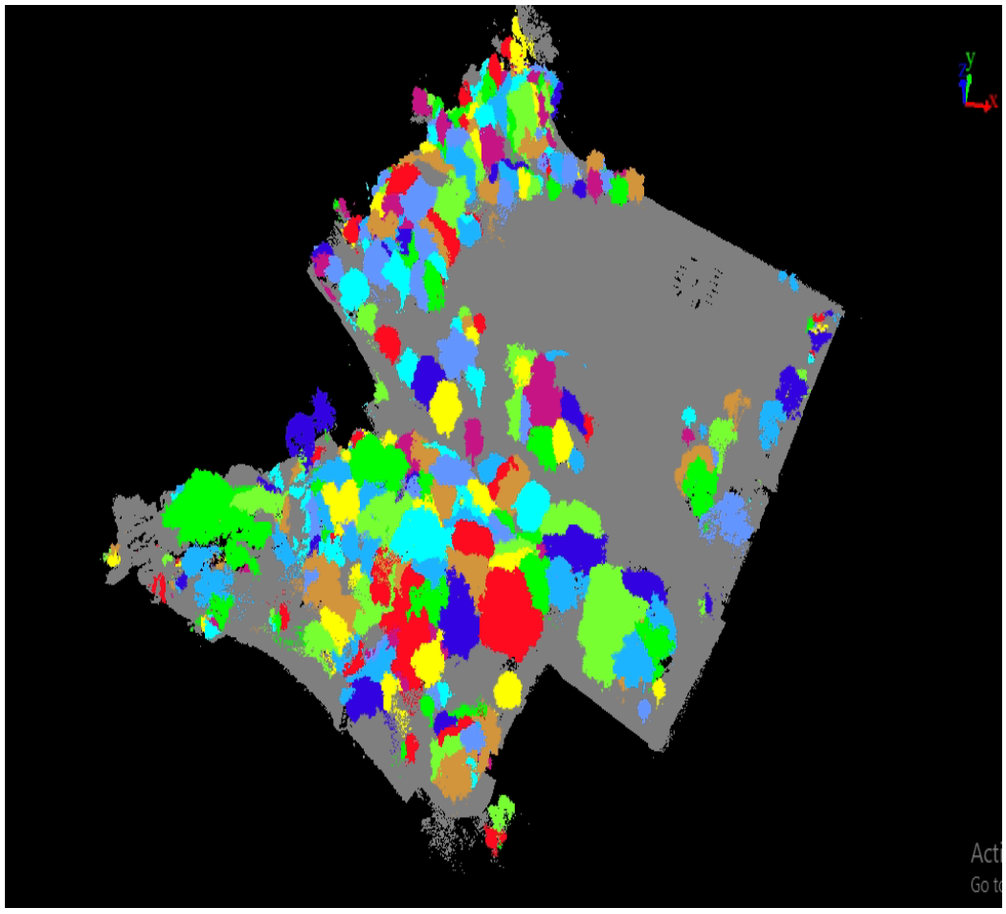

FIGURE 7. The result of individual tree segmentation

TABLE 5. Segmented tree count and its bias.

Segmented tree count	Bias (number of trees)	Relative Bias (%)
191	52	37.4

Individual tree delineation can be seen with a segmentation bias of 52, which is an underestimation of the original manually counted individual trees. Trees can be seen having mixed segmentations with each other. Since the algorithm used is distance-based, it is sensitive to heavily entangled tree crowns. This, combined with the problem of having a high amount of environmental noise from surrounding humans, vehicles, and buildings, poses a challenge in urban forest environments, especially in bustling areas such as the one where the study is taking place.

INDIVIDUAL TREE MEASUREMENT

This subsection exhibits the results gained from the individual tree measurement extraction. Once the individual trees have been delineated, the algorithm clearly establishes the boundaries between them, paving the way for the extraction of measurements. The separation between each tree trunk and the canopy of individual trees allows for more precise measurement. The measurements will cover both plot level and stand level, looking into the likes of diameter at breast height (DBH), individual tree height, and crown diameter for plot level measurements. The results are compared between three different experimental setups, in which each setup has different combinations of parameters. Each LiDAR-derived individual tree measurement will be compared to its corresponding reference data. Quantitative statistics are conducted, namely RMSE, MBE, and the coefficient of correlation (r). Table 6 shows the data validation for each measurement involved in this study.

TABLE 6. Error metrics for the validation of individual tree measurement

Measurement	RMSE(m)	MBE(m)	r
Diameter at breast height	0.107	0.003	0.929
Individual tree height	1.385	-0.636	0.972
Tree crown diameter	2.650	-0.001	0.881

Individual tree measurements consist of individual tree height, diameter at breast height and crown diameter. As mentioned, they are extracted using distinct methods, such as measuring from end-to-end of a tree delineation for individual tree height and tree crown diameter and the circle fitting method for diameter at breast height. These methods produce RMSE of 0.107m, 1.385m and 2.65m for diameter at breast height, individual tree height and tree crown diameter respectively. Note that each of the measurements is attributed directly to the individual tree delineation. Therefore, even with the complete set of points for a single tree, attention should be given to the parameters of the delineation approach. Meanwhile, diameter at breast height registers an acceptable amount of error. Meanwhile, the MBE of diameter at breast height, individual tree height and tree crown diameter are 0.003 m, -0.636 m and -0.001 m respectively. Lower MBE measures might be attributed to their balance of errors between overestimation and underestimation. Meanwhile, individual tree height reported a greater MBE value, signalling an underestimation of tree height at -0.636 m. Meanwhile, the coefficient of correlation (r) is generally high and positive. Therefore, it can be interpreted as each of the measurements having a high and direct correlation between LiDAR-derived measurements and reference measurements.

INDIVIDUAL ABOVEGROUND BIOMASS AND CARBON STOCK ESTIMATION

The individual tree biomass is often calculated from allometric models from other researchers. The current Above ground biomass model is based on an allometric model that involves DBH as an input parameter (Ngo & Lum, 2018). Meanwhile, the carbon stock is the product of above ground biomass and its conversion factor of 0.5 (Lin et al. 2016). Table 7 displays the accuracy metrics for AGB estimation and the accuracy metrics for carbon stock estimation.

TABLE 7. Error metrics for the validation of above ground biomass estimation and carbon stock estimation

Aboveground Biomass		
RMSE (kg)	MBE (kg)	r
1970.24	140.02	0.922
Carbon stock		
RMSE (kg C)	MBE (kg C)	r
886.61	63.01	0.922

Since the input parameter is only the diameter at breast height, the accuracy of AGB and carbon stock is directly linked to the accuracy of the DBH. The RMSE of both above ground biomass and carbon stock are 1970.24 kg and 866.61 kg respectively. It is anticipated that both estimations are sensitive to the change in DBH. The smallest difference in DBH would affect largely on the RMSE measure. Meanwhile, MBE for above ground biomass and carbon stock only experiences 140.02 kg and 63.01 kgC each. Both estimations have overestimation biases similar to DBH's MBE measure. Coefficient of correlation (r) for both estimations is practically the same with a strong and direct relationship with their reference counterparts due to their direct conversion.

CONCLUSION

In this study, we investigate the capabilities of point cloud integrated from multiple point cloud resources. namely,

terrestrial laser scanning (TLS), aerial photogrammetry, UAV-based LiDAR, for individual tree measurements and individual tree biomass and carbon stock estimation. Each of the LiDAR modes was utilized to capture dense point clouds over an urban forest area. The data collection was done across different sensors, which produced different point cloud densities. The point clouds were preprocessed and integrated. It provides a more complete point cloud of each individual trees. The combined point cloud was used to outline individual trees. Next, DBH, tree height and crown diameter were extracted based on the delineated point cloud. The results obtained show a relatively low RMSE measure, indicating the low variability of the lidar derived measurement. Meanwhile, tree measurements experience a general overestimation, and the r value exhibits the integrated point cloud's reliability in characterizing individual trees physical features. Finally, biomass and carbon storage estimations derived from DBH.

Despite a decent output, the limitations of the study must be acknowledged. The study was conducted in a limited area with excessive noise from unrelated objects such as humans, vehicles, and buildings. This affected the integration algorithm due to its nature, which involves randomly sampled points. Even though an outlier elimination process is carried out, the presence of noise still affects the whole process, which is a challenge when operating LiDAR systems in urban forests. The algorithm for individual tree delineation also raises an issue. It uses an iterative point-based approach with distances as its parameters. In an urban tropical forest setting, the complex and intertwined structure of crowns and branches would depend heavily on the quality of the individual tree delineation. Thus, effecting the individual tree measurement. Therefore, based on these limitations, recommendation for future studies can be proposed. This recommendation includes incorporating better noise removal techniques for urban environment as the noise from a scan is not systematic and random (Jaafar et al. 2018; Wassihun et al. 2019). LiDAR calibration models can be utilized and studied to lessen the errors coming from the individual tree measurement. Furthermore, investigations on the use of deep learning in individual tree delineation can be done to reduce the effects of misdelineation caused by irregular tree structures.

ACKNOWLEDGMENT

The authors would like to thank the Ministry of Higher Education and the Universiti Teknologi Malaysia for providing financial support under the Fundamental Research Grant Scheme (FRGS) FRGS/1/2020/TK02/UTM/02/1 (UTM vote No. R.J130000.7852.5F396).

DECLARATION OF COMPETING INTEREST

None.

REFERENCES

Bello, S. A., Yu, S., Wang, C., Adam, J. M. & Li, J. 2020. Review: Deep learning on 3D point clouds. *Remote Sensing* 12(11): 1729. https://doi.org/10.3390/rs12111729

Bu, G. & Wang, P. 2016. Adaptive circle-ellipse fitting method for estimating tree diameter based on single terrestrial laser scanning. *Journal of Applied Remote Sensing* 10(2): 026040.

Burt, A., Disney, M. & Calders, K. 2018. Extracting individual trees from LiDAR point clouds using treeseg. *Methods in Ecology and Evolution*. https://doi.org/10.1111/2041-210x.13121

Cabo, C., Del Pozo, S., Rodríguez-Gonzálvez, P., Ordóñez, C. & González-Aguilera, D. 2018. Comparing terrestrial laser scanning (TLS) and wearable laser scanning (WLS) for individual tree modeling at plot level. *Remote Sensing* 10(4): 540.

Chen, C., Yang, B., Song, S., Peng, X. & Huang, R. 2018. Automatic clearance anomaly detection for transmission line corridors utilizing UAV-borne LiDAR data. *Remote Sensing* 10(4): 613. https://www.mdpi.com/2072-4292/10/4/613

Duncanson, L., Armston, J., Disney, M., Avitabile, V., Barbier, N., Calders, K., Carter, S. et al. 2019. The importance of consistent global forest aboveground biomass product validation. *Surveys in Geophysics* 40: 979–999.

Ganz, S., Käber, Y. & Adler, P. 2019. Measuring tree height with remote sensing—A comparison of photogrammetric and LiDAR data with different field measurements. *Forests* 10(8): 694.

Goldbergs, G., Maier, S. W., Levick, S. R. & Edwards, A. C. 2018. Efficiency of individual tree detection approaches based on light-weight and low-cost UAS imagery in Australian savannas. *Remote Sensing* 10(2): 161. https://doi.org/10.3390/rs10020161

Gupta, A., Byrne, J., Moloney, D., Watson, S. & Yin, H. 2020. Tree annotations in LiDAR data using point densities and convolutional neural networks. *IEEE Transactions on Geoscience and Remote Sensing*. https://doi.org/10.1109/tgrs.2019.2942201

Hartley, R. J., Jayathunga, S., Massam, P. D., De Silva, D., Estarija, H. J., Davidson, S. J., Wuraola, A. & Pearse, G. D. 2022. Assessing the potential of backpack-mounted mobile laser scanning systems for tree phenotyping. *Remote Sensing* 14(14): 3344.

Hilker, T., Leeuwen, M. v., Coops, N. C., Wulder, M. A., Newnham, G., Jupp, D. L. B. & Culvenor, D. 2010. Comparing canopy metrics derived from terrestrial and airborne laser scanning in a Douglas-fir dominated forest stand. *Trees* 24: 819–832. https://doi.org/10.1007/s00468-010-0452-7

Huang, H., Li, Z., Gong, P., Cheng, X., Clinton, N., Cao, C., Ni, W. & Wang, L. 2011. Automated methods for measuring DBH and tree heights with a commercial scanning LiDAR. *Photogrammetric Engineering & Remote Sensing* 77(3): 219–227.

Jaafar, W. S. W. M., Woodhouse, I., Silva, C. A., Omar, H., Maulud, K. N. A., Hudak, A. T., Klauberg, C., Cardíl, A. & Mohan, M. 2018. Improving individual tree crown delineation and attributes estimation of tropical forests using airborne LiDAR data. *Forests* 9(12): 759. https://doi.org/10.3390/f9120759

Jin, S., Zhang, W., Shao, J., Wan, P., Cheng, S., Cai, S., Yan, G. & Li, A. 2022. Estimation of larch growth at the stem, crown, and branch levels using ground-based LiDAR point cloud. *Journal of Remote Sensing* 2022: 9836979. https://doi.org/10.34133/2022/9836979

Kleinn, C., Magnussen, S., Nölke, N., Magdon, P., Álvarez-González, J. G., Fehrmann, L. & Pérez-Cruzado, C. 2020. Improving precision of field inventory estimation of aboveground biomass through an alternative view on plot biomass. *Forest Ecosystems* 7. https://doi.org/10.1186/s40663-020-00268-7

Krisanski, S., Taskhiri, M. S., Gonzalez Aracil, S., Herries, D. & Turner, P. 2021. Sensor agnostic semantic segmentation of structurally diverse and complex forest point clouds using deep learning. *Remote Sensing* 13(8).

Larjavaara, M. & Muller-Landau, H. C. 2013. Measuring tree height: A quantitative comparison of two common field methods in a moist tropical forest. *Methods in Ecology and Evolution* 4(9): 793–801. https://doi.org/10.1111/2041-210X.12071

Li, W., Guo, Q., Jakubowski, M. K. & Kelly, M. 2012. A new method for segmenting individual trees from the LiDAR point cloud. *Photogrammetric Engineering & Remote Sensing* 78(1): 75–84.

Lin, C., Thomson, G. & Popescu, S. C. 2016. An IPCC-compliant technique for forest carbon stock assessment using airborne LiDAR-derived tree metrics and competition index. *Remote Sensing* 8(6): 528.

Liu, G., Wang, J., Dong, P., Chen, Y. & Liu, Z. 2018. Estimating individual tree height and diameter at breast height (DBH) from terrestrial laser scanning (TLS) data at plot level. *Forests* 9(7): 398.

Mooij, J., Janzing, D., Peters, J. & Schölkopf, B. 2009. Regression by dependence minimization and its application to causal inference in additive noise models. *Proceedings of the 26th Annual International Conference on Machine Learning*, Montreal, Quebec, Canada. https://doi.org/10.1145/1553374.1553470

Moroni, G., Syam, W. P. & Petrò, S. 2014. Performance improvement for optimization of the non-linear geometric fitting problem in manufacturing metrology. *Measurement Science and Technology* 25(8). https://doi.org/10.1088/0957-0233/25/8/085008

Ngo, K. M. & Lum, S. 2018. Aboveground biomass estimation of tropical street trees. *Journal of Urban Ecology* 4(1). https://doi.org/10.1093/jue/jux020

Ojoatre, S., Zhang, C., Hussin, Y. A., Kloosterman, H. E. & Ismail, M. H. 2019. Assessing the uncertainty of tree height and aboveground biomass from terrestrial laser scanner and hypsometer using airborne LiDAR data in tropical rainforests. *IEEE Journal of Selected Topics in Applied Earth Observations and Remote Sensing* 12(10): 4149–4159.

Paris, C., Valduga, D. & Bruzzone, L. 2015. A hierarchical approach to the segmentation of single dominant and dominated trees in forest areas by using high-density LiDAR data. https://doi.org/10.1109/igarss.2015.7325698

Paudel, P., Beckschäfer, P. & Kleinn, C. 2021. Impact of training on different observers in forest inventory. *Banko Janakari*. https://doi.org/10.3126/banko.v31i1.37338

Ramezani, H. & Ramezani, A. 2021. Forest fragmentation assessment using field-based sampling data from forest inventories. *Scandinavian Journal of Forest Research*. https://doi.org/10.1080/02827581.2021.1908592

Saarinen, N., Vastaranta, M., Kankare, V., Tanhuanpää, T., Holopainen, M., Hyyppä, J. & Hyyppä, H. 2014. Urban-tree-attribute update using multisource single-tree inventory. *Forests* 5(5): 1032–1052. https://doi.org/10.3390/f5051032

Shin, P., Sankey, T. T., Moore, M. M. & Thode, A. E. 2018. Evaluating unmanned aerial vehicle images for estimating forest canopy fuels in a ponderosa pine stand. *Remote Sensing* 10(8): 1266. https://doi.org/10.3390/rs10081266

Sibona, E., Vitali, A., Meloni, F., Caffo, L., Dotta, A., Lingua, E., Motta, R. & Garbarino, M. 2016. Direct measurement of tree height provides different results on the assessment of LiDAR accuracy. *Forests* 8(1): 7.

Smistad, E., Falch, T. L., Bozorgi, M., Elster, A. C. & Lindseth, F. 2015. Medical image segmentation on GPUs: A comprehensive review. *Medical Image Analysis* 20(1): 1–18.

Srinivasan, S., Popescu, S. C., Eriksson, M., Sheridan, R. & Ku, N.-W. 2015. Terrestrial laser scanning as an effective tool to retrieve tree level height, crown width, and stem diameter. *Remote Sensing* 7(2): 1877–1896. https://doi.org/10.3390/rs70201877

Tao, S., Wu, F., Guo, Q., Wang, Y., Li, W., Xue, B., Hu, X. et al. 2015. Segmenting tree crowns from terrestrial and mobile LiDAR data by exploring ecological theories. *ISPRS Journal of Photogrammetry and Remote Sensing* 110: 66–76. https://doi.org/10.1016/j.isprsjprs.2015.10.007

Wang, C., Nie, S., Xi, X., Luo, S. & Xiao-feng, S. 2016. Estimating the biomass of maize with hyperspectral and LiDAR data. *Remote Sensing* 9(1): 11. https://doi.org/10.3390/rs9010011

Wang, F. & Zhao, Z. 2017. A survey of iterative closest point algorithm. *2017 Chinese Automation Congress (CAC)*, 20–22 October.

Wassihun, A. N., Hussin, Y. A., Van Leeuwen, L. & Latif, Z. A. 2019. Effect of forest stand density on the estimation of above ground biomass/carbon stock using airborne and terrestrial LiDAR derived tree parameters in tropical rain forest, Malaysia. *Environmental Systems Research* 8: 1–15.

Wieser, M., Mandlburger, G., Hollaus, M., Otepka, J., Glira, P. & Pfeifer, N. 2017. A case study of UAS borne laser scanning for measurement of tree stem diameter. *Remote Sensing* 9(11): 1154. https://doi.org/10.3390/rs9111154

Wilkinson, M. W., Jones, R. R., Woods, C. E., Gilment, S. R., McCaffrey, K. J. W., Kokkalas, S. & Long, J. J. 2016. A comparison of terrestrial laser scanning and structure-from-motion photogrammetry as methods for digital outcrop acquisition. *Geosphere* 12(6): 1865–1880. https://doi.org/10.1130/ges01342.1

Wolter, P., Berkley, E., Peckham, S., Singh, A. & Townsend, P. 2012. Exploiting tree shadows on snow for estimating forest basal area using Landsat data. *Remote Sensing of Environment* 121: 69–79.

Yan, W., Guan, H., Cao, L., Yu, Y., Gao, S. & Lu, J. Y. 2018. An automated hierarchical approach for three-dimensional segmentation of single trees using UAV LiDAR data. *Remote Sensing* 10(12): 1999. https://doi.org/10.3390/rs10121999

Zeng, W., Fu, L., Xu, M., Wang, X., Chen, Z. & Yao, S. 2018. Developing individual tree-based models for estimating aboveground biomass of five key coniferous species in China. *Journal of Forestry Research* 29: 1251–1261.

Zhang, C., Zhou, Y. & Qiu, F. 2015. Individual tree segmentation from LiDAR point clouds for urban forest inventory. *Remote Sensing* 7(6): 7892–7913. https://doi.org/10.3390/rs70607892

Zhang, K., Okazawa, H., Hayashi, K., Hayashi, T., Fiwa, L. & Maskey, S. 2022. Optimization of ground control point distribution for unmanned aerial vehicle photogrammetry for inaccessible fields. *Sustainability* 14(15): 9505.

Zhao, X., Guo, Q., Su, Y. & Xue, B. 2016. Improved progressive TIN densification filtering algorithm for airborne LiDAR data in forested areas. *ISPRS Journal of Photogrammetry and Remote Sensing* 117: 79–91. https://doi.org/10.1016/j.isprsjprs.2016.03.016